Microcavity effects in SiGe/Si heterogeneous nanostructures prepared by electrochemical anodization of SiGe/Si multiple quantum wells

S. W. Pan,[1] B. Zhou,[2] Rui Chen,[1,3] S. Y. Chen,[1,a)] Cheng Li,[1] Wei Huang,[1] H. K. Lai,[1] and H. D. Sun[3]

[1]*Semiconductor Photonics Research Center, Department of Physics, Xiamen University, 422 South Siming Road, Xiamen, Fujian 361005, People's Republic of China*

[2]*Department of Physics and Electronic Information Engineering, Minjiang University, Fuzhou, Fujian 350108, People's Republic of China*

[3]*Division of Physics and Applied Physics, School of Physical and Mathematical Sciences, Nanyang Technological University, Singapore 637371, Singapore*

(Received 7 May 2011; accepted 11 September 2011; published online 16 November 2011)

We present the systematic investigations of the microcavity effects from SiGe/Si heterogeneous nanorods (HNRs) prepared by electrochemical anodization of SiGe/Si multiple quantum wells. Visible photoluminescence (PL) emission with narrow bandwidth is observed because of the wavelength selective effect of the microcavity. The resonance of the microcavity is confirmed by the temperature dependent PL measurement, which is consistent with the prediction from the thermo-optic effect. Furthermore, electroluminescence from the ITO/*i*-SiGe/Si HNR/n^--Si diode shows multiple peak emissions under low current density, which is in good agreement with the PL results. © *2011 American Institute of Physics*. [doi:10.1063/1.3653960]

I. INTRODUCTION

A major obstacle for bulk silicon-based materials is the inability to achieve efficient light emission because of the indirect bandgap, which limits their applications in optoelectronics.[1] One promising strategy to overcome this problem is to reduce the dimension of Si-based semiconductor materials and utilize the quantum confinement effects. Therefore, Si and SiGe nanocrystals (NCs) have drawn considerable research attention.[2,3] Because of the size controllability, the bandgap of the NCs can be continuously tuned from visible to near infrared by size variation.[4] However, it is found that the photoluminescence (PL) emission is very broad and weak because of the surface states and size distribution of the NCs. To tackle these problems, various approaches, such as multilayer structure, template, and optical microcavities, have been adopted to modify and enhance the emission.

As is well known, optical microcavities can confine the light inside small volumes by resonant recirculation, which will significantly modify the emission spectrum, such as light intensity enhancement, spectral narrowing, spatial redistribution of the emission, and alteration of the spontaneous emission rate. Therefore, optical microcavities have been used for high-efficiency light-emitting diodes (LED) and low threshold lasers.[5] Until now, Si-based NC optical microcavities, such as one-dimensional planar microcavities,[6–8] microdisks,[9,10] and photonic crystals,[11] have been proposed to improve the luminescence efficiency of Si NCs.

More recently, we have reported on the mechanism of strain-induced anodization of SiGe/Si multiple quantum wells (MQWs) to form high density SiGe/Si heterogeneous nanorods (HNRs).[12] The nanorods with a density up to 2×10^{11} cm^{-2} and a relatively narrow distribution in size were obtained. In this paper, we investigated the microcavity effects of the SiGe/Si HNR prepared by electrochemical anodization (ECA) of SiGe/Si MQWs. Temperature-dependent resonance of visible emissions were observed and ascribed to the thermo-optic effect (TOE) of the SiGe/Si HNR. Finally, electroluminescence (EL) emission from the ITO/*i*-SiGe/Si HNR/n^--Si diode under low current density was observed.

II. EXPERIMENTAL DETAILS

A. Fabrication of SiGe/Si HNR

The SiGe/Si HNRs were fabricated by ECA of SiGe/Si MQWs. The SiGe/Si MQWs were deposited on *n*-type Si (100) substrate by ultrahigh vacuum chemical vapor deposition (UHVCVD) system with a base vacuum of 5×10^{-8} Pa. The *n*-Si substrate having ⟨100⟩ orientation and 500 μm in thickness was lightly doped (n^-) with a resistivity of $0.1 \sim 1.2$ Ω cm. Two samples were prepared. Sample A consisted of 6 period $Si_{0.87}Ge_{0.13}$/Si MQWs and a final 160-nm-thick Si cap layer, and each period includes 7-nm-thick SiGe and 28-nm-thick Si. Sample B consisted of 16 period $Si_{0.81}Ge_{0.19}$/Si MQWs, and each period includes 7-nm-thick SiGe and 72-nm-thick Si layers. Detailed MQW growth conditions and characterizations are available elsewhere.[12] Subsequently, the ECA was performed on the MQWs by using a mixture of 40% hydrofluoric acid solution and ethanol in a volume ratio of 1:2. Samples A and B were etched with a current density of 20 mA/cm^2 for 8 min and 27 mA/cm^2 for 15 min, respectively.

B. Fabricated device

The ITO/*i*-SiGe/Si HNR/n^--Si diode based on sample A was fabricated with the following procedures. After sample A was ECA etched, a 300-nm *n*-type indium tin oxide (ITO)

a)Author to whom correspondence should be addressed. Electronic mail: sychen@xmu.edu.cn.

film with an area of 4×4 mm^2 was deposited on the top of the surface by electron beam evaporation and formed *i*-type (SiGe/Si) heterogeneous nanorods. It was then annealed at 525 °C for 10 min under N_2 atmosphere. Finally, an Al thin film of 300 nm was deposited on the backside of the n^--Si (100) substrate by magnetron sputtering for ohmic contact.

C. Material characterization

The cross-sectional morphologies of SiGe/Si MQWs before and after ECA were analyzed by scanning electron microscopy (SEM). The optical reflectivity measurements were carried out by a Varian Cary 5000 UV-vis-NIR spectrophotometer operated in the 400–800-nm range. The PL measurements were performed using a cw He–Cd laser emitting at 325 nm as the excitation source. EL measurements were performed under dc-biased conditions. For both PL and EL measurements, the signal was dispersed by a 750-mm monochromator combined with suitable filters and detected by a photomultiplier using the standard lock-in amplifier technique. Electrical characteristics of the device were measured using a Keithley 4200-CSC semiconductor parameter analyzer.

III. RESULTS AND DISCUSSION

A. Morphology of the SiGe/Si HNR

Figures 1(a) and 1(b) show the cross-sectional SEM images of the as-grown and etched sample B ($Si_{0.81}Ge_{0.19}$/Si MQW film), respectively. As can be seen in Fig. 1(a), the average thicknesses of the SiGe and Si layers of the MQWs are ~7 and ~72 nm, respectively, which coincide well with the x-ray diffraction simulation results (not shown). As depicted in Fig. 1(b), etching channels, which are parallel to the growth direction consisting of 16 period $Si_{0.81}Ge_{0.19}$/Si MQWs, can be well resolved. The total thickness of the etched film was ~1678 nm. It should be mentioned that the strain due to the lattice constant difference between SiGe and Si plays a very important role during the etching process, which was discussed in our previous research work.[12] Based on the above SEM results, the heterogeneous nanorods with a uniform size distribution in 3D space have been achieved in our samples. As shown in Fig. 1(c), the porous SiGe/Si HNRs have lower refractive indices (1.93 for Si and 2.25 for SiGe in wavelengths from 600 to 700 nm) than that in bulk Si (3.75).[13,14] Therefore, the two interfaces, the sample surface, and the interface between porous SiGe/Si and Si substrates could be treated as mirrors that form an optical cavity.

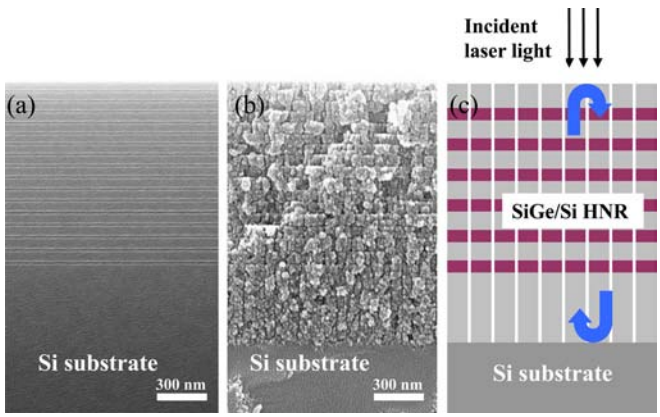

FIG. 1. (Color online) Cross-sectional SEM micrographs from (a) as-UHVCVD grown, and (b) the etched sample B (16 period $Si_{0.8}Ge_{0.2}$/Si MQWs). (c) The sketch of the cavity formed by the mirrors at the surface and the Si substrate interface.

B. Reflectance and photoluminescence of the SiGe/Si HNRs

Figure 2 shows the PL and reflectance spectra of samples A and B after ECA at room temperature. It should be mentioned that there is no emission from the as-grown sample. Therefore, the visible emission from the samples after ECA can be ascribed to porous SiGe/Si HNRs. The periodic peaks displayed in PL from 500 to 800 nm in both samples coincide with the dips in the reflectance spectrum very well. The periodicity of the PL peaks observed in our samples, with the intervals between adjacent PL peaks increasing with wavelength, can be ascribed to the wavelength selective effect of the Fabry-Perot (F-P) cavities.[15,16] Compared with the broad- and single-band emission from porous Si,[17] and porous SiGe alloys,[18] five peaks with narrow linewidths (less than 30 nm) are observed in the two samples, where both of the strongest peaks at 669 nm in sample A and at 644 nm in sample B are labeled "P4."

The spectral characteristics of a cavity are sensitive to the cavity length. Only when the wavelength of the enhanced luminescence obeys Eq. (1) can the luminescence pass through the cavity and be collected:[15,16,19]

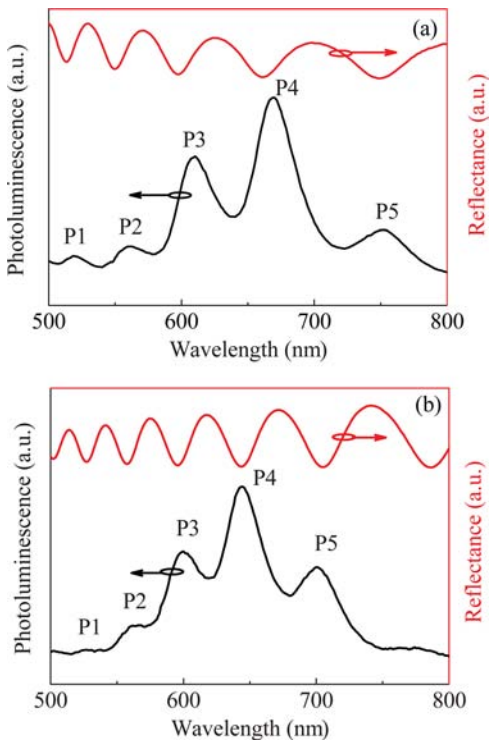

FIG. 2. (Color online) Room-temperature PL and reflectance spectrum from the (a) etched sample A, and (b) and the etched sample B.

$$2\frac{2n\pi}{\lambda}L + \psi_1 + \psi_2 = 2m\pi \quad (m = 1, 2, 3, ...). \tag{1}$$

Here, n is the refractive index, λ is the vacuum wavelength of the PL, L is the cavity length, and ψ_1 and ψ_2 denote phase shifts due to the penetration into the mirrors. The mode numbers of these resonances m were found to range from $m = 13$ ($\lambda_{13} = 519$ nm) to $m = 9$ ($\lambda_9 = 750$ nm) for sample A after ECA, and range from $m = 17$ ($\lambda_{17} = 527$ nm) to $m = 13$ ($\lambda_{13} = 700$ nm) for sample B after ECA. And we obtained the values of n and L as 2.68 and 1258 nm (for the etched sample A), respectively.

That the intervals of the adjacent peaks of the room-temperature PL increase with wavelength is well elucidated by the following free spectral range (FSR) equation,[16,19] which describes the wavelength selective effect of the F-P cavity:

$$FSR = \frac{\lambda^2}{2n_{\text{eff}}L_{\text{eff}}}. \tag{2}$$

Here, λ is the wavelength of the luminescence and n_{eff} and L_{eff} denote the effective refractive index and the effective cavity length, respectively. As shown in Fig. 2, the intervals of the adjacent peaks of the PL are 40 nm, 49 nm, 62 nm, and 79 nm, which are in agreement with Eq. (2). According to this equation, sharp and strong room-temperature PL peaks could be optimized by further tuning the quantum-well structure and anodization parameters.

C. The thermo-optic effect of the SiGe/Si HNRs

To verify the microcavity effect of the emission from SiGe/Si HNRs, PL measurement was carried out at temperatures from 10 to 300 K. Figure 3(a) shows the normalized spectra measured at various temperatures. As the temperature increased from 10 to 300 K, the five peaks (P_1 to P_5) are found to redshift about 8–9 nm. It is noted that the envelopes of the multiple peak emission remain very similar, which indicates that the photon energy of the emission is not changed with temperature. Moreover, the intensity of the emission at 10 K is similar to the room-temperature emission. As is well known, the broad visible emissions from porous Si or SiGe come from surface states that are not sensitive to temperature.[2,20] And it is also found that the size of the SiGe/Si HNRs is too big to introduce the quantum confinement effect. Therefore, the visible emission of the SiGe/Si HNRs is ascribed to the recombination from the interface defect state emission of the sample.

It is also interesting to note that the PL emissions demonstrate a redshift with the temperature. Based on the formula $\lambda = 2nL/m$, converted from Eq. (1), the mode wavelength of the cavity is determined by material refractive index n and cavity length L. Therefore, the thermal sensitivity could be ascribed to the temperature-dependent n and L, because of TOE and the thermal expansion of the SiGe/Si HNRs, respectively. Differentiating Eq. (1) with respect to T yields:

$$\frac{d\lambda}{dT} = \frac{2}{m}\left(n\frac{dL}{dT} + L\frac{dn}{dT}\right), \tag{3}$$

where the term $L(T) = L(1 + \alpha\Delta T)$ and $n(T) = n + \beta\Delta T$ are the temperature-dependent cavity length and the refractive index, respectively. α and β are the thermal expansion and thermo-optic coefficient, respectively. So we obtain

$$\lambda(T) = \frac{2Ln}{m} + \frac{2L}{m}(\beta + \alpha n)\Delta T + \frac{2L}{m}\alpha\beta\Delta T^2. \tag{4}$$

For crystalline Si (and Ge), the values of α and β are 2.6×10^{-6} K^{-1} (and 5.9×10^{-6} K^{-1}) and 1.86×10^{-4} K^{-1} (and 3.5×10^{-4} K^{-1}), respectively. So β accounts for approximately 96% contribution to the observed wavelength shift.[21–24] Thus, in SiGe/Si HNR, the wavelength shift with temperature can be approximately given by:

$$\lambda(T) = \frac{2Ln}{m} + \frac{2L\beta}{m}\Delta T. \tag{5}$$

Figure 3(b) illustrates the peak wavelength of sample A after ECA as a function of temperature. From the best fit of the experimental data, the parameters obtained are $n = 2.68$ and $\beta = 1.36 \times 10^{-4}K^{-1}$ (at 300 K), which are very close to the previous reports.[14,25] Therefore, it can be concluded that the

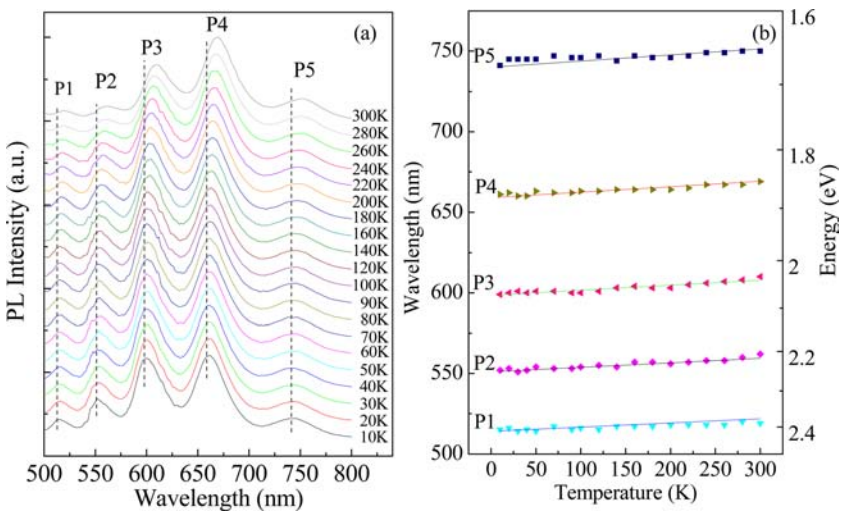

FIG. 3. (Color online) (a) Normalized temperature-dependent PL spectra of sample B from 10 to 300 K. (b) Temperature-dependent peak wavelength (or energies) and solid lines are the fitting of the experimental data based on Eq. (5).

temperature-induced refractive index change in the SiGe/Si HNR is the main factor that is responsible for the thermal variation in the resonator behavior.

D. Electroluminescence of the ITO/*i*-SiGe/Si HNR/n^--Si diode

Typical *I–V* characteristics of the ITO/*i*-SiGe/Si HNR/n^--Si diode based on sample A after etching are depicted in Fig. 4. Nonlinear behaviors are observed at both forward and reverse biases. The turn-on voltages are ~0.47 and 1.45 V under forward and reverse biases, respectively. This indicates that the n^--Si substrate has a lower conduction-band energy difference with *i*-SiGe/Si HNRs, favoring the electron injection from Si to *i*-SiGe/Si HNRs.

The EL spectra of the ITO/*i*-SiGe/Si HNR/n^--Si diode recorded at room temperature under various forward injection currents densities are shown in Fig. 5, whereas no EL is detected under reverse bias. In the case of forward bias, electrons injected from ITO to *i*-SiGe/Si HNRs can radiatively recombine with holes injected from n^--Si to *i*-SiGe/Si HNRs. It is known that *n*-type substrates are poor providers of holes. However, for our devices, it should be mentioned that the n^--Si substrate was lightly doped with a doping concentration of $\sim 10^{15}$ cm^{-3}, which makes the voltage mainly fall on the substrate. Under positive bias, the energy bands of n^--Si will bend upward, which induces an inversion layer near the interface between the n^--Si substrate and the *i*-SiGe/Si HNR. Moreover, the valence band of n^--Si [E_V(Si)] will move down under positive bias, which results in hole accumulations at the interface. When sufficient bias is applied, the E_V(Si) level will be even lower than the acceptor level of the *i*-SiGe/Si HNR interface state. Therefore, those accumulated holes at the interface will be able to tunnel into the *i*-SiGe/Si HNRs through the barrier and recombine with the electrons to generate the visible emission. In comparison, for the case of reverse bias, although there is no problem for the electrons existing in *i*-SiGe/Si HNRs, the higher Schottky barrier between ITO and *i*-SiGe/Si HNRs prevents the injection of holes. This is the reason why no EL signal was detected when a negative voltage was applied to the Si substrate. As shown in Fig. 5, a series of periodic peaks in the range of 500–900 nm were observed, which is in agreement with the result of PL. The positions of all the peaks remain

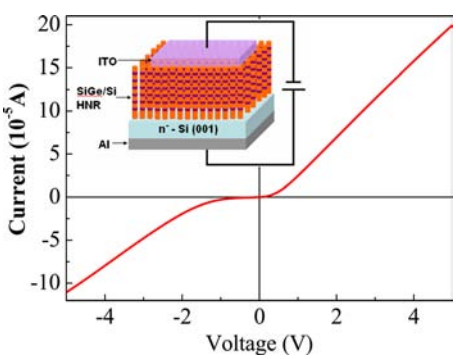

FIG. 4. (Color online) *I–V* characteristics of the ITO/*i*-SiGe/Si HNR/n^--Si diode; the area of the diode is 4×4 mm^2. The inset shows the schematic diagram of the device.

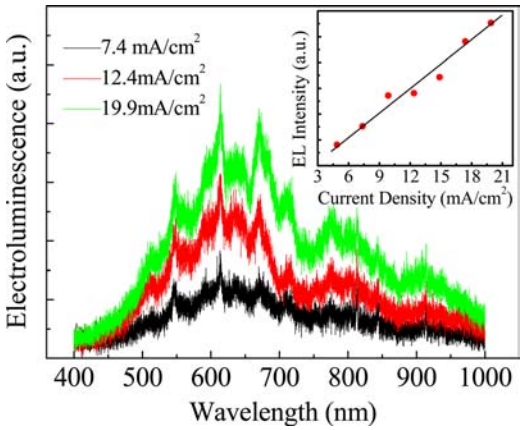

FIG. 5. (Color online) Room-temperature EL spectra of the ITO/*i*-SiGe/Si HNR/n^--Si diode device under various current densities. The inset shows the integrated EL intensity of the devices as a function of injection current density.

unchanged under different injection current densities. The integrated EL intensity of the device as a function of injection current density was shown in the inset of Fig. 5. Linear behavior was observed at forward biases, which indicates that most of the injected carriers are recombined radiatively. Although the efficiency of the device is not high, our results provide a proof-of-concept demonstration that a proper microcavity can not only considerably increase the external efficiency of luminescence in SiGe/Si heterogeneous nanostructures, but also decrease the bandwidth and selectively tune the peak wavelength for Si based devices.

IV. CONCLUSIONS

We report the observation of EL and PL from the microcavity structures containing SiGe/Si HNRs prepared by ECA of SiGe/Si MQWs. Strong luminescence spectra with multiple peaks and narrow widths in both EL and PL are observed. Temperature-dependent PL peak position indicates that the TOE of the SiGe/Si HNR plays a predominant role in governing temperature-dependent resonance wavelengths.

ACKNOWLEDGMENTS

This work is supported by the Nation Natural Science Foundation of China under Grant Nos. 61176050, 61036003, 61176092, and 60837001 (Key Program). The National Basic Research Program of China under Grant No. 2012CB933503 and the Fundamental Research Funds for the Central Universities (2010121056). The Foundation of Education Committee of Fujian Province (JB10124, JB11128), and the Technology Startup Project of Minjiang University (KQ1004).

[1]M. A. Green, J. H. Zhao, A. H. Wang, P. J. Reece, and M. Gal, Nature **412**, 805 (2001).
[2]X. X. Wang, J. G. Zhang, L. Ding, B. W. Cheng, W. K. Ge, J. Z. Yu, and Q. M. Wang, Phys. Rev. B **72**, 195313 (2005).
[3]S. Takeoka, K. Toshikiyo, M. Fujii, S. Hayashi, and K. Yamamoto, Phys. Rev. B **61**, 15988 (2000).
[4]D. Y. Chen, Y. Liu, J. Xu, D. Y. Wei, H. C. Sun, L. Xu, T. Wang, W. Li, and K. J. Chen, Opt. Express **18**, 917 (2010).

[5]R. Chen, H. D. Sun, T. Wang, K. N. Hui, and H. W. Choi, Appl. Phys. Lett. **96**, 241101 (2010).
[6]F. Iacona, G. Franzò, E. C. Moreira, and F. Priolo, J. Appl. Phys. **89**, 8354 (2001).
[7]A. Belarouci and F. Gourbilleau, J. Appl. Phys. **101**, 073108 (2007).
[8]S.-Y. Seoa and K. J. Kim, J. Appl. Phys. **106**, 076103 (2009).
[9]R. J. Zhang, S. Y. Seo, A. P. Milenin, M. Zacharias, and U. Gösele, Appl. Phys. Lett. **88**, 153120 (2006).
[10]R. D. Kekatpure and M. L. Brongersma, Nano Lett. **8**, 3787 (2008).
[11]C. D. Presti, A. Irrera, G. Franzò, I. Crupi, F. Priolo, and F. Iacona, Appl. Phys. Lett. **88**, 033501 (2006).
[12]B. Zhou, S. W. Pan, R. Chen, S. Y. Chen, C. Li, H. K. Lai, J. Z. Yu, and X. F. Zhu, Solid State Commun. **149**, 1897 (2009).
[13]C. Mazzoleni and L. Pavesi, Appl. Phys. Lett. **67**, 2983 (1995).
[14]K. Toshikiyo, M. Fujii, and S. Hayashi, J. Appl. Phys. **93**, 2178 (2003).
[15]A. Serpengüzel, A. Aydinli, A. Bek, and M. Güre, J. Opt. Soc. Am. B **15**, 2706 (1998).
[16]C. B. Li, B. W. Cheng, R. W. Mao, Y. H. Zuo, W. H. Shi, C. J. Huang, L. P. Luo, J. Z. Yu, and Q. M. Wang, Thin Solid Films **467**, 197 (2004).
[17]S. Y. Chen, Y. H. Huang, H. K. Lai, C. Li, and J. Y. Wang, Solid State Commun. **142**, 358 (2007).
[18]A. Ksendzov, R. W. Fathauer, T. George, W. T. Pike, R. P. Vasquez, and A. P. Taylor, Appl. Phys. Lett. **63**, 200 (1993).
[19]M. S. Ünlü and S. Strite, J. Appl. Phys. **78**, 607 (1995).
[20]M. L. Brongersma, P. G. Kik, A. Polman, K. S. Min, and H. A. Atwater, Appl. Phys. Lett. **76**, 351 (2000).
[21]Y. Okada and Y. Tokumaru, J. Appl. Phys. **56**, 314 (1984).
[22]S. I. Novikova, Fiz. Tverd. Tela **2**, 43 (1960) [Sov. Phys.-Solid State **2**, 37 (1960)].
[23]G. Cocorullo, F. G. C. Della, and I. Rendina, Appl. Phys. Lett. **74**, 3338 (1999).
[24]G. D. Gillen and S. Guha, Appl. Opt. **44**, 344 (2005).
[25]S.-Y. Seo, J. Lee, J. H. Shin, E.-S. Kang, and B.-S. Bae, Appl. Phys. Lett. **85**, 2526 (2004).